Stator Current Vector Determination Under Consideration of Local Iron Loss Distribution for Partial Load Operation of PMSM

Andreas Ruf, Simon Steentjes, Andreas Thul, and Kay Hameyer, *Senior Member, IEEE*

***Abstract*—Iron losses have a large share in the overall losses of high power density electrical machines operating as variable speed drives. Especially in the partial load area, the ratio of iron losses is dominant with respect to the copper losses. Therefore, commonly used control strategies, such as maximum torque per ampere or maximum torque per voltage, aiming at minimizing the current for given restrictions as the maximum voltage do not select the best direct and quadrature currents to maximize the efficiency or minimize the overall losses at each operating point. This paper elaborates a stator current vector determination strategy considering the iron loss distribution at all operating points, comparing different iron loss models in a machine with distributed windings. Depending on the operating point and the operational conditions of the machine, the overall losses can be reduced up to 7%.**

***Index Terms*—Efficiency optimization, field oriented vector control, loss minimization, nonlinear optimization.**

I. Introduction

PERMANENT-MAGNET synchronous machines (PMSM) are used in electrical drive trains requiring high power density and high efficiency in a wide operating range. Especially PMSM with buried magnets offer high power densities and low rotor losses. The magnetic saliences leads to a reluctance torque which can be used applying the best direct and quadrature (dq) current combination to maximize the torque per ampere (MTPA). This results in minimal copper losses and is a common choice. However, in high power density machines operating as variable speed drives iron losses have a large share in various operating points due to high magnetic utilization and elaborated field frequencies. On that account, the iron losses need to be considered in all operating points to select the best direct and quadrature current combination leading to the lowest overall losses. For this purpose, the iron loss calculation scheme is of particular interest. This loss minimizing control strategy is known as the maximum efficiency (ME) control, whose theory is well known and has been proposed and applied by different authors [1]–[3].

A commonly used approach to represent the variability of the iron losses is to add a speed-dependent iron loss equivalent resistance to the machine model [1], [2], [4]–[7] or to employ variable loss coefficients [8] and elementary iron loss models [9]–[13]. All of these approaches solely consider iron losses caused by the fundamental harmonic of the magnetic flux density in the machine leading to a strong simplification, in particular in the field-weakening range.

The main challenge and central task of the loss minimizing control strategy is an accurate description of the considered loss components maintaining the simplicity of the loss models to be applicable for real-time applications. Depending on whether or not a prototype exists, the loss models are parametrized by measurements [11], [14] or directly lookup tables of measured losses are used to accomplish the simplicity and accuracy [8]. Considering the speed-dependent additional losses during the control of the machine enables to minimize the overall losses, tantamount to maximizing the efficiency. For PMSM especially at the partial load area the efficiency can be improved, because at this area the iron losses are dominant. Considering the drive cycles of speed-variable traction drives in [8] and [14] show that the average efficiency gain or energy loss decrease rises up to 2 %, which is a non-negligible amount that can be achieved by the correct control of the machine.

This paper deals with the same methodical approach to minimize the overall losses, but in contrast to other investigations, this paper bases the iron loss estimation solely on standardized Epstein measurement data to parametrize the applied iron loss models in combination with a finite-element model and specific control strategy to incorporate the operation characteristics of the machine. This approach allows combining efficiently the material information gained from standardized measurements (loss and nonlinear magnetization behavior) and the operation dependent load characteristics. Therewith, an *a priori* design and loss prediction of the machine across the whole torque–speed map is possible. The importance of the used iron loss model and the comparison with measured data is discussed in detail. This paper uses two extended iron loss models [15] in combination with finite-element simulations to derive a more accurate loss minimizing control strategy. These two extended iron loss models share an additional eddy-current loss component to account for increased iron losses at high magnetic flux densities and high excitation frequencies. They are different in terms of the

Manuscript received June 01, 2015; revised September 17, 2015 and November 21, 2015; accepted December 28, 2015. Date of publication April 06, 2016; date of current version July 15, 2016. Paper 2015-EMC-0297.R2, presented at the 2015 IEEE International Electric Machines and Drives Conference, Coeur d'Alene, ID USA, May 10–13, and approved for publication in the IEEE Transactions on Industry Applications by the Electric Machines Committee of the IEEE Industry Applications Society.

The authors are with the Institute of Electrical Machines, RWTH Aachen University, Aachen 52062, Germany (e-mail: Andreas.Ruf@iem.rwth-aachen.de; Simon.Steentjes@iem.rwth-aachen.de; Andreas.Thul@iem.rwth-aachen.de; Kay.Hameyer@iem.rwth-aachen.de).

Color versions of one or more of the figures in this paper are available online at http://ieeexplore.ieee.org.

Digital Object Identifier 10.1109/TIA.2016.2549991

consideration of higher harmonic flux density component and the hysteresis loss component.

II. Modeling Approach

A. Machine Model

In order to evaluate the proposed methodology a PMSM machine with buried magnets (see Table II) is modeled in a rotor-flux-fixed dq-reference frame including cross coupling magnetization and saturation [16]

$$\begin{bmatrix} \hat{\Psi}_{\mathrm{d}} \\ \hat{\Psi}_{\mathrm{q}} \end{bmatrix} = \begin{bmatrix} L_{\mathrm{dd}} & L_{\mathrm{dq}} \\ L_{\mathrm{qd}} & L_{\mathrm{qq}} \end{bmatrix} \begin{bmatrix} \hat{i}_{\mathrm{d}} \\ \hat{i}_{\mathrm{q}} \end{bmatrix} + \begin{bmatrix} \hat{\Psi}_{\mathrm{f,d}} \\ \hat{\Psi}_{\mathrm{f,q}} \end{bmatrix}. \tag{1}$$

The quadrature and direct current is varied during simulation to extract the torque calculated by the eggshell method for different excitation [17]. The average torque is determined by the formula

$$T = \frac{3}{2} p \left(\hat{\Psi}_{\mathrm{d}} \hat{i}_{\mathrm{q}} - \hat{\Psi}_{\mathrm{q}} \hat{i}_{\mathrm{d}} \right). \tag{2}$$

To calculate the efficiency of the machine, the various loss components which occur during the operation have to be considered. These are detailed in the following sections.

B. Copper Loss Model

For the consideration of the copper or ohmic losses, the equation

$$P_{\mathrm{Cu}} = 3 R_{\mathrm{s}}(\theta) i_{\mathrm{eff}}^2$$

is used. The influence of the changing temperature of the stator windings is taken into account using a temperature dependent stator resistance $R_{\mathrm{s}}(\theta)$, which is calculated by

$$R_{\mathrm{s}}(\theta) = R_{\mathrm{s}}(\theta_0) \cdot (1 + \alpha_{20} (\theta - \theta_0)). \tag{3}$$

The resistance $R_{\mathrm{s}}(\theta_0)$ is determined by a dc measurement at temperature θ_0 and for the simulation results set to a fixed value at temperature $\theta = 100\ ^{\circ}\mathrm{C}$ with the temperature coefficient $\alpha_{20} = 3.9 \cdot 10^{-3}\ \mathrm{K}^{-1}$. Comparing the simulation results with measurement results, the temperature of the winding is considered. Additional copper losses due to eddy currents and inverter loss are not taken into account.

C. Iron Loss Model

The utilized iron loss model [15] is critical to this control strategy. The model is critical to deliver reliable and accurate results in all operating points of the machine, i.e., material saturation characteristics, rotational iron losses, and harmonics need to be considered. Based on this, the loss distribution can be calculated and the control strategy adjusted. In this paper, two different iron loss calculation methods are applied. The first one calculates the iron losses solely based on the fundamental component of the magnetic flux density B_1 in combination with the fundamental frequency f_1. More precisely, the Fourier summations in (5) to (8) are replaced by the fundamental components. The second approach considers the influence of induced field harmonics using a Fourier series representation of the magnetic flux density waveform for the least common multiple of an electrical period and the rotational period of the rotor. Based on this, the amplitudes and orders of the field harmonics can be used for the iron loss calculation [18]–[20]. The level of magnetic flux distortion and rotational magnetization are included in both models in a similar way using the maximal and minimal magnetic flux densities B_{max}, i.e., B_{min}, over the finite elements of the machine model during one magnetic period

TABLE I
Iron Loss Model Coefficients for the Investigated Electrical Steel, Classified as M330-35A

α	a_1	a_2	a_3	a_4	a_5
2.0	$18.531e^{-3}$	$62.75e^{-6}$	$32.55e^{-3}$	5.0	$0.4e^{-3}$

$$P_{\mathrm{Fe}} = P_{\mathrm{hyst}} + P_{\mathrm{classical}} + P_{\mathrm{excess}} + P_{\mathrm{sat}} \tag{4}$$

with the following loss contributions:

$$P_{\mathrm{hyst}} = a_1 \left(1 + \frac{B_{\mathrm{min}}}{B_{\mathrm{max}}} (r_{\mathrm{hyst}} - 1) \right) B_{\mathrm{max}}^{\alpha} f_1 \tag{5}$$

$$P_{\mathrm{classical}} = a_2 \sum_{n=1}^{\infty} \left(B_n^2 (n f_1)^2 \right) \tag{6}$$

$$P_{\mathrm{excess}} = a_5 \left(1 + \frac{B_{\mathrm{min}}}{B_{\mathrm{max}}} (r_{\mathrm{excess}} - 1) \right) \times \sum_{n=1}^{\infty} \left(B_{\mathrm{n}}^{1.5} (n f_1)^{1.5} \right) \tag{7}$$

$$P_{\mathrm{sat}} = a_2 a_3 B_{\mathrm{max}}^{a_4 + 2} f_1^2 \tag{8}$$

where $\frac{B_{\mathrm{min}}}{B_{\mathrm{max}}}$ represents the ratio of minimal and maximal magnetic flux density amplitudes over one magnetic period and r_{hyst} as well as r_{excess} the rotational loss factor [15]. Considering the flux distortion factor, arbitrary spatial flux density loci can be described. The second component considers the classical Foucault eddy current losses and takes harmonics into account. Hereby, a summation over all n harmonics is conducted. The same is performed for the third, the excess loss component. Thereby B_{n} represent the amplitude of the n-th harmonic.

The material dependent parameters ($a_1 - a_5$ and α) of the iron loss model (see Table I) are identified using standardized Epstein measurement data (purely sinusoidal magnetic flux density waveforms).

These parameters are adjusted to account for occurring deterioration effects due to induced mechanical stresses. In order to map the effect of mechanical stress due to cutting into the iron loss estimation scheme used for machine calculation, the hysteresis losses which are most prone to manufacturing processing are modified using the overall cut edge length per unit mass being a measure of the induced cutting stress instead of using empirical building factors [21], [22]. This approach was validated using a loss parameter set solely based on single sheet tester measurements of samples with varying proportion of cutting surface per unit volume [22] and applied in this paper using Epstein datasets.

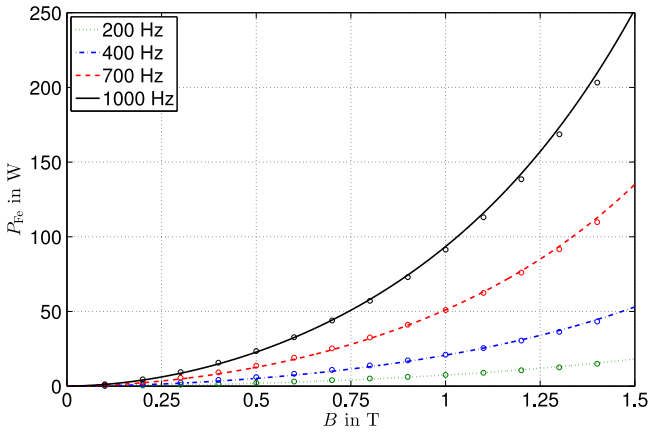

Fig. 1. Comparison of calculated iron losses (lines) with measurements (dots) at different frequencies using parameters of Table I for material grade M330-35A.

A comparison of loss predictions and measurements is depicted in Fig. 1.

D. Bearing Loss Model

The losses due to friction occurring in the shaft bearings are modeled by using an analytic approach

$$P_{\mathrm{bear}} = n_{\mathrm{bear}} f_0 \left(v_{\mathrm{bear}} n\right)^{\frac{2}{3}} d_{\mathrm{bear}}^3 \cdot 2\pi n \cdot 10^{-7}$$

where n_{bear}, f_0, v_{bear}, and d_{bear} denominate the number of bearings, the bearing coefficient, the bearing viscosity, and the bearing diameter. Values for f_0 and v_{bear} are taken for the data sheets provided by the bearing manufacturer. They are both temperature dependent and set to a mean value depending on the operating conditions.

III. Model-Based Control Strategies

In order to calculate the operation points for the entire operating range, a combined control strategy is used. The optimization problem is defined by

$$\underset{\hat{i}_{\mathrm{d},i,j},\hat{i}_{\mathrm{q},i,j}\in\mathbb{R}}{\text{minimize}} \quad J(\hat{i}_{\mathrm{d},i,j},\hat{i}_{\mathrm{q},i,j}) = \sqrt{\hat{i}_{\mathrm{d},i,j}^2 + \hat{i}_{\mathrm{q},i,j}^2}$$

$$\text{subject to} \quad T_{\mathrm{i}} = \frac{3}{2} p \left(\hat{\Psi}_{\mathrm{d,i}}\hat{i}_{\mathrm{q,i}} - \hat{\Psi}_{\mathrm{q,i}}\hat{i}_{\mathrm{d,i}}\right) \quad \forall\, i = 1,\ldots,m$$

$$\hat{u}_{\mathrm{j}} = \omega_{\mathrm{j}}\hat{\Psi}_{\mathrm{i}} \leq \hat{u}_{\max} \quad \forall\, j = 1,\ldots,n.$$

with the torque vector $T_1, T_2, \ldots, T_{\mathrm{m}}$ subject to $m \in \mathbb{N}$ and the speed vector $n_1, n_2, \ldots, n_{\mathrm{n}}$ with $n \in \mathbb{N}$. This optimization problem combines the MTPA control for the base speed range and the maximum torque per voltage (MTPV) control for the flux weakening range. This control strategy minimizes the current vector, which is tantamount to minimized ohmic losses. Since the current amplitudes are known, which is the case for current driven controls, this control scheme is a simple method to reduce the losses and maximize the efficiency. However, this control strategy neglects the other losses, which are influenced by the direction and amplitude of the current vector. Due to the current-dependent magnetic field distribution the iron losses

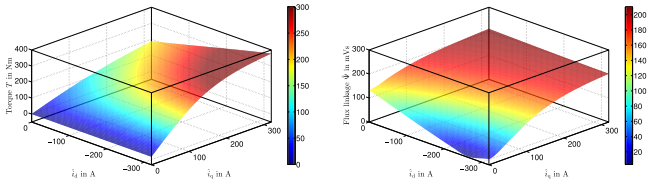

(a) Average torque vs. $\hat{i}_{\mathrm{d}}, \hat{i}_{\mathrm{q}}$. (b) Flux linkage vs. $\hat{i}_{\mathrm{d}}, \hat{i}_{\mathrm{q}}$.

Fig. 2. Torque and flux-linkage in dq-reference frame. (a) Average torque versus $\hat{i}_{\mathrm{d}}, \hat{i}_{\mathrm{q}}$. (b) Flux linkage versus $\hat{i}_{\mathrm{d}}, \hat{i}_{\mathrm{q}}$.

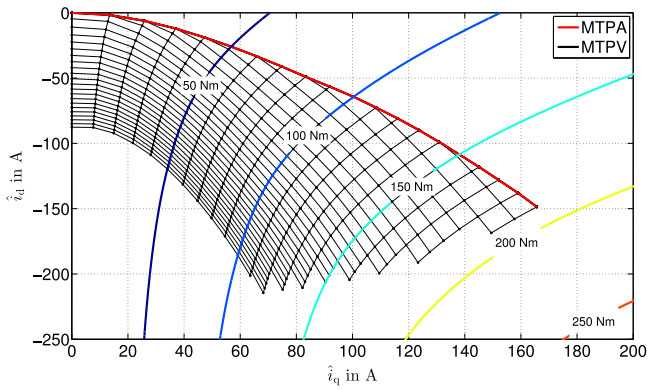

Fig. 3. MTPA-trajectory versus $\hat{i}_{\mathrm{d}}, \hat{i}_{\mathrm{q}}$.

are also dependent on the position of the current vector for each occurring frequency. For this reason the iron losses can be considered in the control strategy by

$$\underset{\hat{i}_{\mathrm{d},i,j},\hat{i}_{\mathrm{q},i,j}\in\mathbb{R}}{\text{minimize}} \quad J(P_{\mathrm{Loss},i,j}) = P_{\mathrm{Cu},i,j} + P_{\mathrm{fe},i,j}$$

$$\text{subject to} \quad T_{\mathrm{i}} = \frac{3}{2} p \left(\hat{\Psi}_{\mathrm{d,i}}\hat{i}_{\mathrm{q,i}} - \hat{\Psi}_{\mathrm{q,i}}\hat{i}_{\mathrm{d,i}}\right), \quad \forall\, i = 1,\ldots,m$$

$$\hat{u}_{\mathrm{j}} = \omega_{\mathrm{j}}\hat{\Psi}_{\mathrm{i}} \leq \hat{u}_{\max}, \quad \forall\, j = 1,\ldots,n.$$

This optimization problem combines the maximum torque per loss (MTPL) control or the ME control for the base speed range and the MTPV control for the flux weakening range and it has the same boundary conditions as the MTPA control.

IV. Results

A. Simulation Results

Fig. 2 presents the result of the calculated average torque and flux-linkage for different dq-current excitations using finite-element simulation. In the case of a PMSM with buried magnets, it is shown that the torque and the flux strongly depend on the magnitude and angle of the rotor-flux-fixed current vector. This current-dependent data can be used by the first control strategy to calculate the speed–torque depended operating points.

Fig. 3 shows the trajectories of the average electro-magnetic torque calculated with different current excitations. Further, an overlapping mesh of calculated operating points, from 0 to 400 Hz fundamental electrical frequency and 0 to 190 Nm inner electro-magnetic torque, using the combined control strategy is mapped. The rotor-flux-fixed current vectors are defined for each operating point by the operation points, which

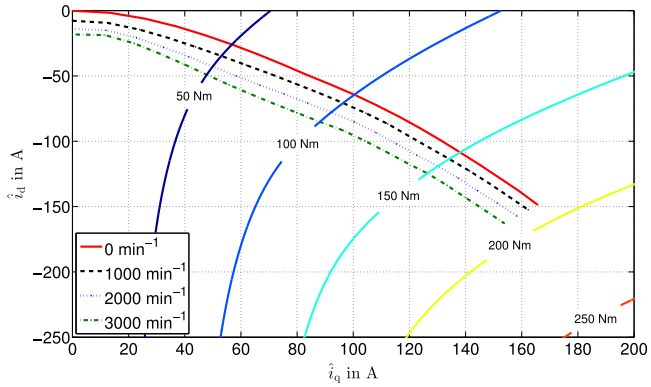

Fig. 4. MTPL-trajectory versus $\hat{i}_\mathrm{d}, \hat{i}_\mathrm{q}$.

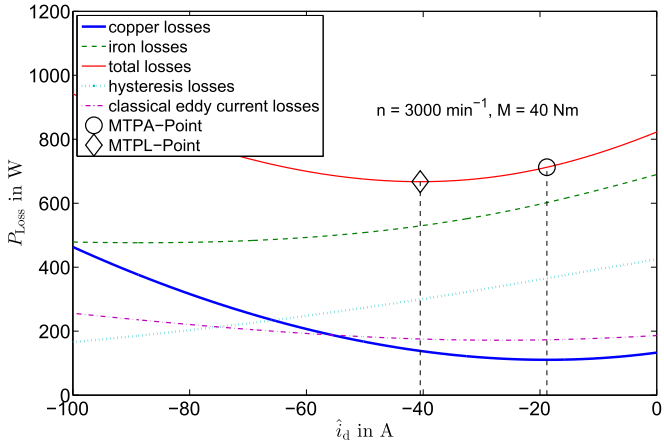

Fig. 5. Loss distribution versus the d-axis current ($n = 3000$ min^{-1}).

are calculated for the given optimization problem. The basic speed range is represented by the trajectory that extends along the rising torques (red), whereas the flux weakening area is represented by the mesh below this trajectory.

In comparison to these results, Fig. 4 presents the operating points for the overall loss minimizing MTPL control strategy. For the MTPA control, all operation points for different frequencies in the base frequency range are on the MTPA-trajectory (red) until the voltage limit is reached, because only the current is considered and minimized by this strategy. As soon as the voltage limit is reached, the operating points are frequency dependent due to the additional flux weakening. This operation area is, for both control strategies, the same, because the voltage limit is in both cases the dominant factor or boundary and the point of minimum current as well as the point of minimum losses are out of the possible current excitations. The MTPL control strategy can exclusively be applied in the base speed range. In Fig. 4, the MTPL-trajectories for four different velocities are presented. At standstill, the trajectory corresponds to the MTPA-trajectory. With elevated speed, the trajectories move to the negative d-axis, i.e., the flux weakening to reduce the flux density and the occurring iron losses to accomplish the point of minimum losses. Points of operation can be realized by different current excitations along the trajectories for given torques and speeds (see Figs. 5 and 6). It is apparent that the point of

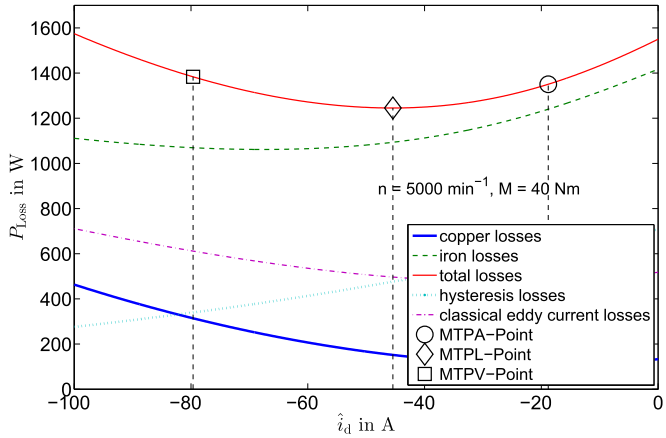

Fig. 6. Loss distribution versus the d-axis current ($n = 5000$ min^{-1}).

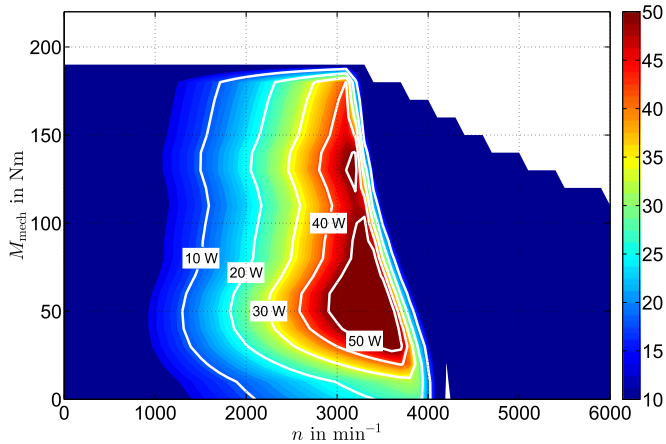

Fig. 7. Absolute reduced sum of losses in W using MTPL.

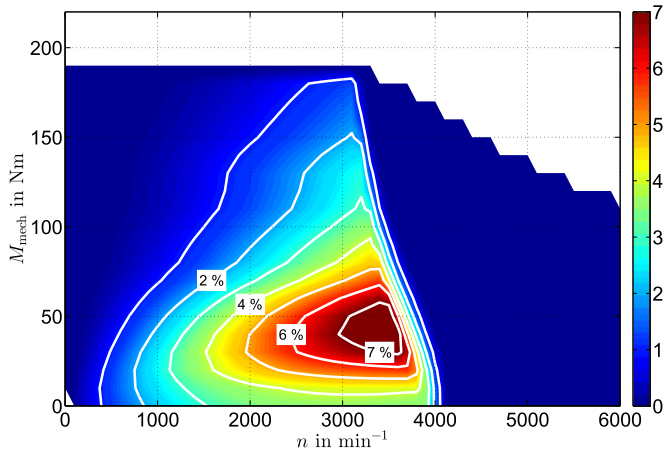

Fig. 8. Relative reduced sum of losses in % using MTPL.

minimum losses is shifted to the direction of the negative d-axis. By decreasing the hysteresis loss by flux weakening, the higher field harmonics can cause an increase of eddy current losses, which need to be considered to minimize the overall losses. The result of reducing losses for all operation is presented in Figs. 7 and 8. The maximum reduction of losses primarily depends on the voltage limit, which is also shown in Fig. 6. As soon as

TABLE II
SIMULATION AND MACHINE PARAMETERS OF THE IPMSM

Magnet material	NdFeB
Number of Poles/Slots $2p/N$	8/48
Winding configuration	Distributed winding
Stator outer radius $r_{\mathrm{stator,o}}$	135 mm
Rotor outer radius $r_{\mathrm{rotor,o}}$	80 mm
Axial length l_{Fe}	90 mm
Air gap length δ	0.7 mm
Battery voltage U_{dc}	400 V
Rated current I_{n}	142 A
Rated torque M_{n}	162 Nm
Rated speed n_{n}	2500 min^{-1}
Rated power P_{n}	42.4 kW

the voltage limit is reached, the MTPV criteria is the dominant factor for adjusting the dq-current combination. Fig. 8 presents the relative reduced sum of losses in % using the following formula:

$$p_{\%} = \frac{P_{\mathrm{MTPA}} - P_{\mathrm{MTPL}}}{P_{\mathrm{MTPL}}}.$$

The area which is reached just before the voltage limit is the most influenced area by the loss minimizing strategy. In particular, the partial load area, where the iron losses are dominant, the efficiency is increased. For this machine this method achieves the best results between 3000 and 4000 min^{-1}.

B. Experimental Results

The machine under test is an eight-pole synchronous machine with V-shape internal permanent magnets (IPMSM), dimensions and electrical parameters are given in Table II. The load machine is a speed controlled induction servo motor. A torque transducer (HBM T12) is coupled between the machine under test and the load machine. The power analyzer (Yokogawa WT 1800) is used to calculate the electrical input power. The power analyzer additionally calculates the mechanical power transmitted between the machine under test and the load machine using the torque transmitter. Thus, the overall power losses in the machine under test can be determined. As the iron losses cannot be measured directly, an accurate copper loss calculation is important for a proper iron loss separation. Therefore, the temperature in the stator winding is measured at different positions to evaluate the average temperature. The initial magnet temperature is measured using a rotating telemetry and has a value of 51 °C. During the measurements of the maps presented below, the induced voltage is measured in the no load case to evaluate the temperature change of the magnets. The change in the induced voltage in no load operation is below 0.9 %, what indicates a temperature change of below 10 K. Comparing measurements with simulations, the temperature of magnets in the simulation is kept constant at 55 °C.

Fig. 9 presents the measured points (black) and the interpolated temperature in the end winding of the stator during the following analyzed measurement. Using (3), the temperature-dependent stator resistance value can be calculated for each measurement. In addition, the mechanical losses through bearings are calculated with Section II-D. Since these are small compared

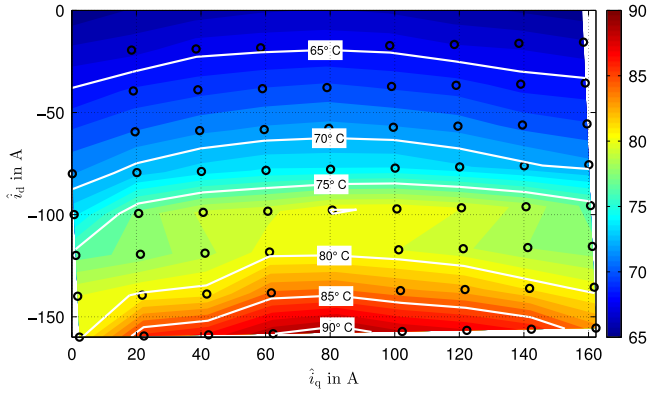

Fig. 9. Stator winding temperature during measurement.

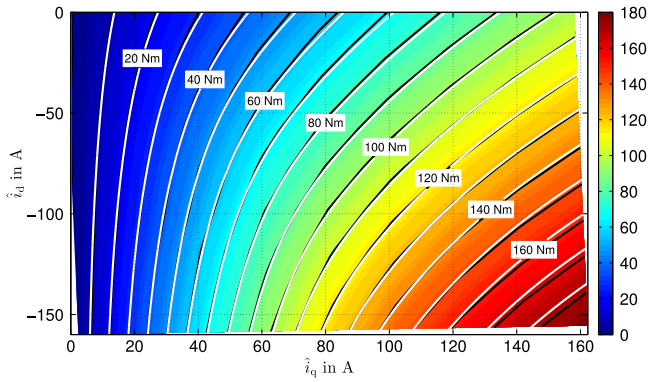

Fig. 10. Comparison of measured (black) and simulated (white) torque.

to the copper and iron losses, the mean measured temperature is used for approximating the bearing coefficients. Since the simulation results indicated that the maximum achievable loss reduction can be achieved for operating points located close to the maximum inverter voltage (between 3000 and 4000 r/min) as shown in Figs. 7 and 8, a fixed speed of 3000 r/min is chosen, where the voltage limit does not reach the maximum voltage for all current vectors. The reference speed is controlled by the load machine. For the MUT a grid of reference values is defined in the dq-current plane, as indicated by the black dots in Fig. 9. For each quadrature current value, the direct current is varied. To keep the temperature changes caused by high currents as small as possible, small and large reference current values are set alternately. As seen in Fig. 9, the temperature change during the measurement is limited to 30 K using this procedure. The change in rotor temperature, which affects a change in the permanent magnet flux density and further a change in the induced voltage, torque, and iron losses. During the measurement, the induced voltage is evaluated after each step in no load tests to keep the change in the voltage and temperature low. To avoid multiple FE simulations, the mean value of the measured induced voltage is used to adapt the flux linkage in the simulation.

Figs. 10 and 11 present a comparison between measured (black) and simulated (white) torque and flux linkage values in the dq-reference current plane, which indicates a good correlation between the measured values and this simplification. In order to achieve a good match between the measured flux link-

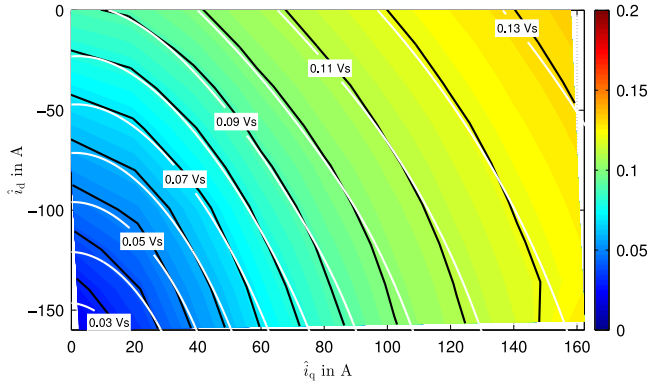

Fig. 11. Comparison of measured (black) and simulated (white) flux linkage.

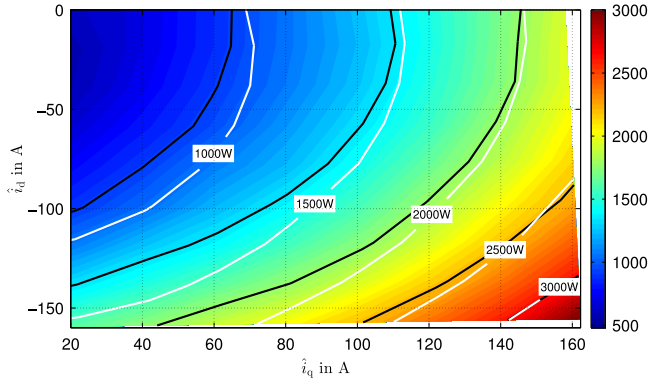

Fig. 13. Comparison of measured (black) and simulated (white) losses (without harmonics).

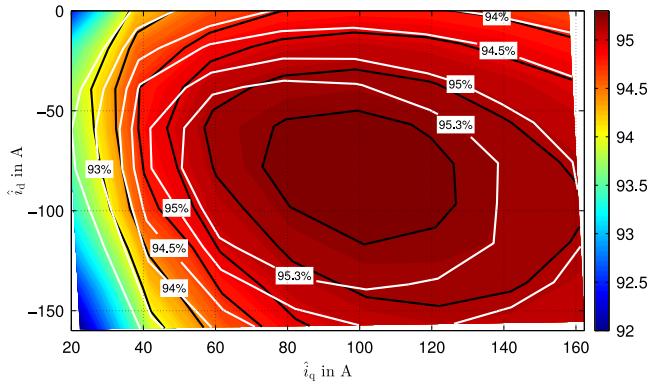

Fig. 12. Comparison of measured (black) and simulated (white) efficiency (without harmonics).

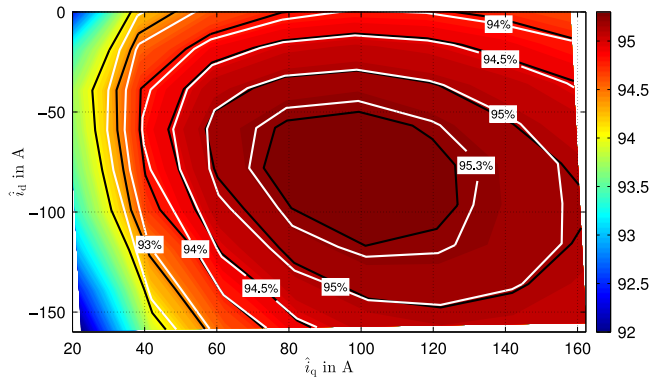

Fig. 14. Comparison of measured (black) and simulated (white) efficiency (including harmonics).

age and the simulation results, the machine model described in (1) must be extended by a leakage inductance. This leakage inductance is determined by parameter variation during post processing and set to the value $L_\sigma = 50\,\mu$H. The result of the adaptation is shown in Fig. 11. This shows in the whole dq-reference plane a good match. After this adaptation, the machine can be controlled by the MTPA/MTPV control using the dq-current depended flux linkage and torque. For the loss minimizing control MTPL, the losses must be known. For the copper loss model, the stator resistance and the temporary winding temperature have to be measured and it is simple to calculate the ohmic losses occurring in the winding. For higher electric frequencies additional losses by eddy currents have to be considered in this model. The knowledge about the temporary occurring iron losses is not as simple. In this paper, two models are used to compare the utility for the loss minimizing control. As described, the two models are parameterized by measurements at the Epstein frame. In order to determine the losses occurring in the machine, the difference between the supplied electric power and the mechanical power is calculated. The measured efficiency (black) is presented for 3000 r/min in Figs. 12 and 14. The first comparison between measured and simulated results using the first iron loss model, without considering the harmonics in the flux density, is presented in Figs. 12 and 13. The results show a good match in the direction of the quadrature current and a nearly good match of the point of ME. In the direction of the negative direct current the consistency of measured (black) and simulated (white) results is poor. The simulated efficiency is too high in the greatest part of the measurement and increases in the direction of the d-axis. This is a result of the underestimated losses in the flux weakening area, which can be seen in Fig. 13. The measured and simulated data have a good match for high d- and q-currents but decreases in the partial load area. As shown in the simulated results, the area of partial load is the most important area for the loss minimizing control, because in this area the iron losses are the dominant loss part, which has to be minimized.

Adding the iron losses produced by the harmonics in the flux density leads to a significant improvement of the data match. Especially the efficiency comparison in Fig. 14 shows an excellent match of the measured and simulated data. The point of ME can be calculated more precisely. In particular flux weakening area in negative d-axis show a high improvement comparing to the first approach with the iron loss model without harmonics. Fig. 15 presents the comparison between measured and simulated losses. This approach shows a good match between measured and simulated losses. Comparing to the first approach, the losses increase in the whole dq-plane and are particularly severe in the flux weakening area. However, this approach shows an overestimation of the iron losses near the d-axis. Building the difference of the two iron loss simulation approaches delivers the part of losses produced by harmonics in Fig. 16. The

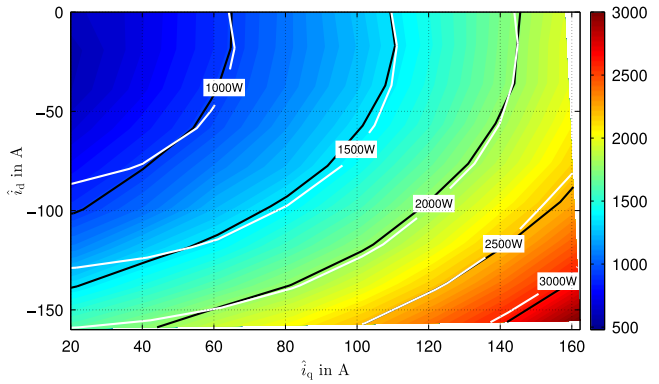

Fig. 15. Comparison of measured (black) and simulated (white) losses (including harmonics).

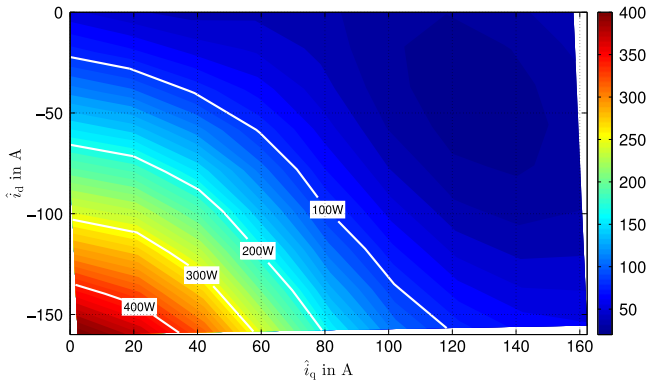

Fig. 16. Simulated iron losses caused by harmonics.

calculated iron losses increase in the negative d-axis, which is in contrast to the behavior of the flux linkage.

V. Conclusion

In this paper, a methodology to reduce the overall losses in arbitrary operating points is proposed. Central part of this loss minimizing control strategy represents the simultaneous consideration of occurring copper losses and current dependent iron loss distribution. It is shown that this approach can be used to calculate the loss distribution *a priori* using iron loss models which are parameterized utilizing standardized Epstein measurement data adapted to account for the internal mechanical stress due to cutting using the relation of the cutting surface to the overall sample volume.

The used iron loss model is the most influencing parameter for the loss minimizing control strategy and should consider material saturation characteristics, rotational iron losses, and harmonics to deliver reliable and accurate results in all operating points. The loss minimizing control reduces hysteresis losses by adding a direct or flux weakening current component. This increases the ohmic losses but also the classical current losses, due to field harmonics, which has to be considered in the iron loss computation. In this paper, an iron loss model is used, which considers the influence of induced field harmonics using a Fourier series representation of the magnetic flux density waveform for the least common multiple of an electrical period and the rotational period of the rotor. This approach shows a good validation with measured data. The interdependence of macroscopic and microscopic eddy currents, hysteresis, skin-effect, and magnetic saturation significantly affects the field distribution within the lamination and as a consequence, the overall iron losses and magnetizability. FE-Modells using the same *BH*-curve for all simulated frequencies do not consider the field and harmonics reducing skin effect. Therefore, frequency-dependent magnetization characteristics are used to map the effect of eddy currents. Uncertain factors, such as high frequency loss in windings, eddy current loss in magnets, temperature depended magnet flux, temperature depended loss parameters, and uncertain factors in the loss parameters make the maximum efficiency control challenging in practical use. In conclusion, this approach shows a methodology for *a priori* loss prediction using standardized Epstein measurement data to parametrize iron loss models to obtain the current combinations, which minimize the overall losses in each operating point.

References

[1] F. Fernandez-Bernal, A. Garcia-Cerrada, and R. Faure, "Determination of parameters in interior permanent-magnet synchronous motors with iron losses without torque measurement," *IEEE Trans. Ind. Appl.*, vol. 37, no. 5, pp. 1265–1272, Sep. 2001.

[2] G.-X. Zhou, H.-J. Wang, D.-H. Lee, and J.-W. Ahn, "Study on efficiency optimizing of PMSM for pump applications," in *Proc. 7th Int. Conf. Power Electron.*, Oct. 2007, pp. 912–915.

[3] J. Lee, K. Nam, S. Choi, and S. Kwon, "A lookup table based loss minimizing control for fcev permanent magnet synchronous motors," in *Proc. IEEE Veh. Power. Prop. Conf.*, Sep. 2007, pp. 175–179.

[4] M. Cao and N. Hoshi, "Electrical loss minimization strategy for interior permanent magnet synchronous motor drives," in *Proc. IEEE Veh. Power Prop. Conf.*, Sep. 2010, pp. 1–6.

[5] J. Stumper, A. Dotlinger, J. Jung, and R. Kennel, "Predictive control of a permanent magnet synchronous machine based on real-time dynamic optimization," in *Proc. 14th Eur. Conf. Power Electron. Appl.*, Aug. 2011, pp. 1–8.

[6] T. Windisch and W. Hofmann, "Loss minimization of an ipmsm drive using pre-calculated optimized current references," in *Proc. 37th Annu. Conf. IEEE Ind. Electron. Soc.*, Nov. 2011, pp. 4704–4709.

[7] S. Odhano, R. Bojoi, A. Boglietti, G. Griva, and S. Rosu, "Maximum efficiency per torque direct flux vector control of induction motor drives," in *Proc. IEEE Energy Convers. Congr. Expo.*, Sep. 2014, pp. 1293–1300.

[8] J. Goss, M. Popescu, D. Staton, R. Wrobel, J. Yon, and P. Mellor, "A comparison between maximum torque/ampere and maximum efficiency control strategies in IPM synchronous machines," in *Proc. IEEE Energy Convers. Congr. Expo.*, Sep. 2014, pp. 2403–2410.

[9] J. Lee, K. Nam, S. Choi, and S. Kwon, "Loss-minimizing control of PMSM with the use of polynomial approximations," *IEEE Trans. Power Electron.*, vol. 24, no. 4, pp. 1071–1082, Apr. 2009.

[10] C. Mademlis and N. Margaris, "Loss minimization in vector-controlled interior permanent-magnet synchronous motor drives," *IEEE Trans. Ind. Electron.*, vol. 49, no. 6, pp. 1344–1347, Dec. 2002.

[11] D. Pohlenz and J. Böcker, "Efficiency improvement of an ipmsm using maximum efficiency operating strategy," in *Proc. 14th Int. Power Electron. Motion Control Conf.*, Sep. 2010, pp. T5-15–T5-19.

[12] C. Mademlis and N. Margaris, "Loss minimization in vector-controlled interior permanent-magnet synchronous motor drives," *IEEE Trans. Ind. Electron.*, vol. 49, no. 6, pp. 1344–1347, Dec. 2002.

[13] H. Aorith, J. Wang, and P. Lazari, "A new loss minimization algorithm for interior permanent magnet synchronous machine drives," in *Proc. IEEE Int. Elect. Mach. Drives Conf.*, May 2013, pp. 526–533.

[14] A. Rabiei, T. Thiringer, and J. Lindberg, "Maximizing the energy efficiency of a PMSM for vehicular applications using an iron loss accounting optimization based on nonlinear programming," in *Proc. XXth Int. Conf. Elect. Mach.*, Sep. 2012, pp. 1001–1007.

[15] S. Steentjes, M. Lessmann, and K. Hameyer, "Advanced iron-loss calculation as a basis for efficiency improvement of electrical machines in automotive application," in *Proc. Elect. Syst. Aircraft, Railway Ship Prop.*, Oct. 2012, pp. 1–6.
[16] T. Herold, D. Franck, E. Lange, and K. Hameyer, "Extension of a d-q model of a permanent magnet excited synchronous machine by including saturation, cross-coupling and slotting effects," in *Proc. IEEE Int. Elect. Mach. Drives Conf.*, May 2011, pp. 1363–1367.
[17] F. Henrotte, G. Deliége, and K. Hameyer, "The eggshell approach for the computation of electromagnetic forces in 2D and 3D," *COMPEL*, vol. 23, no. 4, pp. 996–1005, 2004.
[18] G. Bertotti, A. Canova, M. Chiampi, D. Chiarabaglio, F. Fiorillo, and A. Rietto, "Core loss prediction combining physical models with numerical field analysis," *J. Magn. Magn. Mater.*, vol. 133, pp. 647–650, 1994.
[19] F. Fiorillo and A. Novikov, "An improved approach to power losses in magnetic laminations under nonsinusoidal induction waveform," *IEEE Trans. Magn.*, vol. 26, no. 5, pp. 2904–2910, Sep. 1990.
[20] F. Fiorillo and A. Novikov, "Power losses under sinusoidal, trapezoidal and distorted induction waveform," *IEEE Trans. Magn.*, vol. 26, no. 5, pp. 2559–2561, Sep. 1990.
[21] S. Steentjes, G. von Pfingsten, and K. Hameyer, "An application-oriented approach for consideration of material degradation effects due to cutting on iron losses and magnetizability," *IEEE Trans. Magn.*, vol. 50, no. 11, pp. 1–4, Nov. 2014.
[22] G. von Pfingsten, S. Steentjes, A. Thul, T. Herold, and K. Hameyer, "Soft magnetic material degradation due to manufacturing process: A comparison of measurements and numerical simulations," in *Proc. 17th Int. Conf. Elect. Mach. Syst.*, Oct. 2014, pp. 2018–2024.

Andreas Ruf received the M.Sc. degree in electrical engineering from Ruhr University Bochum (RUB), Bochum, Germany, in 2012.

He has been working as a Research Associate with the Institute of Electrical Machines, RWTH Aachen University, Aachen, Germany, since January 2013. His research interests include iron loss computations, thermal behavior, overload capability, lifetime models, and the design and control of electrical machines.

Simon Steentjes eceived the diploma degree in electrical engineering from RWTH Aachen University, Aachen, Germany, in 2011.

He has been working as a Research Associate with the Institute of Electrical Machines, RWTH Aachen University, since December 2011. His research interests include hard- and soft magnetic material modeling on the micro- and macroscopic scale, iron loss calculation, effects of material processing, magnetic forces, and mathematical methods.

Andreas Thul received the diploma degree in electrical engineering from RWTH Aachen University, Aachen, Germany, in 2013.

He has been working as a Research Associate with the Institute of Electrical Machines, RWTH Aachen University, since October 2013. His research interests include control of electrical machines, electric linear motors, and measurement techniques for the characterization of soft magnetic materials.

Kay Hameyer (M'96–SM'99) received the M.Sc. degree in electrical engineering from the University of Hannover, Hannover, Germany, in 1986, and the Ph.D. degree in permanent magnet excited machines from the University of Technology Berlin, Berlin, Germany, in 1992.

After his university studies, he worked at Robert Bosch GmbH, Stuttgart, Germany, as a Design Engineer for permanent magnet servo motors. From 1988 to 1993, he was a Member of Staff at the University of Technology Berlin. From 1996 to 2004, he was a Full Professor of Numerical Field Computations and Electrical Machines at Katholieke Universiteit Leuven (KU Leuven), Leuven, Belgium. Since 2004, he has been a Full Professor and the Director of the Institute of Electrical Machines (IEM), RWTH Aachen University, Aachen, Germany. His research interest focuses on all aspects of the design, control, and manufacturing of electrical machines and the associated numerical simulation. The characterization and modeling of hard- and soft-magnetic materials is another focus of his work. He has authored/co-authored more than 250 journal publications, more than 500 international conference publications, and four books. His research interests include numerical field computation and optimization, and the design and control of electrical machines, in particular, permanent-magnet excited machines and induction machines.

Dr. Hameyer has been a member of the German VDE since 2004, and a fellow of the Institution of Engineering and Technology, U.K., since 2002.